The influence of synoptic circulations and local processes on temperature anomalies in three French observatories

Cheikh DIONE[1*†], Fabienne LOHOU[1], Marjolaine CHIRIACO[2], Marie LOTHON[1], Sophie BASTIN[2], Jean-Luc BARAY[3], Pascal YIOU[4] and Aurélie COLOMB[3]

(1) Laboratoire d'Aérologie, Université de Toulouse, CNRS, UPS, France.

(2) LATMOS/IPSL, UVSQ Université Paris-Saclay, UPMC Univ. Paris 06, CNRS, Guyancourt, France.

(3) Laboratoire de Météorologie Physique, UMR 6016 Université Blaise Pascal/CNRS, Clermont Ferrand, France.

(4) Laboratoire des Sciences du Climat et de l'Environnement, UMR8212 CEA-CNRS-UVSQ, Université Paris - Saclay & IPSL, Gif-Sur-Yvette, France.

[*] *Corresponding author address:* Dr. Cheikh DIONE, Centre de Recherches Atmosphériques, 8 route de Lannemezan, 65300 Campistrous, France.

E-mail: Cheikh.dione@aero.obs-mip.fr

[†] Current affiliation: Laboratoire d'Aérologie, Université de Toulouse, CNRS, UPS, France.

ABSTRACT

The quantification of the relative contribution of the synoptic-scale circulation relative to that of local and mesoscale processes concerning the variability of middle latitude temperature anomalies was investigated from 2003 to 2013. Meteorological variables collected from three French observatories and from reanalyses were used. Four weather regimes were defined from sea level pressure anomalies from NCEP reanalyses with a K-means algorithm. No correlation was found between the daily temperature anomalies and the weather regimes and the variability of temperature anomalies within each regime is large. It was therefore not possible to evaluate the effect of the large scale on the temperature anomalies by this method. An alternative approach was found with the use of the analogues method: the principle being that for each day of the considered time series, a set of days which had a similar large-scale 500 hPa geopotential height field within a fixed domain were considered. The observed temperature anomalies were then compared to those observed during the analogue days: the closer the two types of series, the greater the mark of the large scale. This method highlights a widely predominant influence of the large scale atmospheric circulation on the temperature anomalies. It showed a potentially larger influence of the Mediterranean Sea and orographic flow on the two southern observatories. Low-level cloud radiative effects were also found to be able to greatly modulate the variability of the daily temperature anomalies.

1. Introduction

The temperature fluctuations of France and, more generally, Western European are largely connected to large-scale weather regimes. However, the processes linking atmospheric variability to surface temperature may vary with the season. Cattiaux et al. (2010) used the geopotential height at 500 hPa to define weather regimes influencing Europe and found that the cold winter of 2010 was associated with a large occurrence of the negative phase of the North Atlantic Oscillation (NAO) weather regime. In summer, major heat waves over France and the UK are generally linked to persisting anticyclonic conditions (such as those in 2003) (Cassou et al. 2005; Yiou et al. 2008). They may also be linked to Atlantic low pressure, which leads to southerly flows (such as those seen in 2015), with amplification by soil moisture-temperature and boundary layer feedbacks (Schär et al. 2004; Seneviratne et al. 2006; Fischer et al. 2007b; Vautard et al. 2007; Quesada et al. 2012; Miralles et al. 2014). Warm winters are linked to a zonal westerly flow (such as in 2007 and 2014) (Luterbacher et al. 2007), which can be amplified by land albedo and cloud radiative effects. The role of such amplifying factors was investigated mainly with regional model simulations (Zampieri et al. 2009; Stegehuis et al. 2013; Seneviratne et al. 2004; Stefanon et al. 2014), but it was proven necessary to use high resolution observations to validate such an approach, since models seemed to exacerbate the role of these factors over Europe (Cheruy et al. 2014; Bastin et al. 2016). For example, Chiriaco et al. (2014), using a combination of space and ground-based observations and twin simulations, showed that the heat wave that occurred over Northern Europe in July 2006 was linked to specific large-scale conditions favoring a low cloud deficit over this area and was amplified by dry soil, which contributed to about 40% of the anomaly.

As for the weather regimes, the large scale flow analogues method was also used to study the seasonal variability of surface temperature anomalies over Europe (Cattiaux et al. 2010; Chiriaco et al.

2014; Vautard and Yiou 2009; Yiou et al. 2007). Cattiaux et al. (2010) found a positive departure of observed temperatures from flow analogues larger for minimal than for maximal temperatures. They observed the maximal departure over the Alps region. Spatial variability and underestimation of the observed temperature anomalies by the reconstructed temperature anomalies suggest an important role of the smaller scale processes concerning temperature anomalies. France is located in a transitional region between the subtropical influence and Atlantic perturbations. It covers an area where climatic models predict a large dispersion in temperature and precipitations due to different sensitivities to local processes (Boé and Terray 2014). For these reasons, it is useful to employ observational data to quantify the influence of large-scale atmospheric circulations relative to those of local processes on the variability of daily temperature anomalies across France.

Our study aims to quantify the relative contributions of large-scale atmospheric circulations and of local processes on the variability of temperature anomalies in three observatories located in France. For this, we shall evaluate specific issues : (i) the effect of the weather regimes on daily temperature anomalies by use of the classification of weather regimes defined from sea level pressure (Yiou and Nogaj 2004), and (ii) the capability of local processes to amplify or reduce temperature anomalies by use of flow analogue atmospheric circulations based on the geopotential height at 500 hPa (Yiou et al. 2007). Our analysis is based on a series of meteorological variables (temperature, wind and radiation) observed in three observatories from ROSEA (Réseau d'Observatoires pour la Surveillance de l'Eau Atmosphérique) national network. It is also based on reanalyses (NCEP and ECMWF).

The manuscript is organized as follows. In section 2, the three ROSEA observatories, the corresponding datasets, the large-scale diagnostic and the methodological approach are presented. Section 3 presents the analysis of large-scale conditions versus local processes using flow analogues. Conclusions appear in section 4.

2. Data and methodology

a. Observatories

In this study, we use the surface observations of three observatories (SIRTA (Site Instrumental de Recherche en Télédetection Active), COPDD (Cézeaux-Opme-Puy De Dôme) and P2OA (Plateforme Pyrénéenne de l'Observation de l'Atmosphère)) from the five ROSEA network observatories, located across varied landscapes along a North-South transect across France (Figs. 1a and 1b).

1) SIRTA

The northern observatory of ROSEA is known as SIRTA (48.7°N-2.2°E and 160 m elevation) (Haeffelin 2005). SIRTA is located on a plateau in a suburban area in Palaiseau, 20 km southwest of Paris (Fig. 1a). It is an instrumental site dedicated to the research into physical and chemical processes in the atmosphere, mainly using remote sensing. Since 2002, observations of precipitation, water vapor, clouds, meteorological variables, atmospheric gases, solar radiation, and wind power have been collected. More details concerning the SIRTA observatory can be found in Haeffelin (2005) or on the following website: http://sirta.ipsl.polytechnique.fr/sirta.old/. Quality control and homogenization of the data in an hourly time-resolution was undertaken at SIRTA for the entire observation period (Chiriaco et al. 2014; Cheruy et al. 2013). This project, named SIRTA-ReOBS, provides a single netCDF file with more than 40 variables from 2003 to 2013 (http://sirta.ipsl.polytechnique.fr/sirta.old/reobs.html).

2) CÉZEAUX-COPDD

The COPDD observatory is located in the Auvergne region, in the center of France (Fig. 1a) where various in situ and remote sensing instruments continuously measure the atmospheric dy-

namics, radiation, atmospheric gases, cloud microphysical variables and aerosols. This observatory is composed of three instrumental sites: Cézeaux (at an altitude of 394 m, an urban site, Opme (at an altitude of 680 m), and Puy-De-Dôme (at an altitude of 1465 m). In this study, we use the meteorological variables collected at the Cézeaux site in order to obtain relatively similar terrain across the three sites. The Cézeaux site (45.47°N-3.05°E) is located on a plain on the campus of Blaise Pascal University in Clermont Ferrand. Since 2002, meteorological variables have been measured at this site. More details concerning the COPDD observatory can be found on the following website; http://wwwobs.univ-bpclermont.fr/SO/mesures/index.php.

3) CRA-P2OA

The P2OA observatory is the south most site (Fig. 1a). It is located in the Midi-Pyrenées region and is composed of two sites from the Observatoire Midi Pyrénées (OMP): the Atmospheric Research Center (CRA) in Lannemezan (43.13°N-0.369°E at an altitude of 600 m), and the "Pic du Midi" (43.13°N-0.37°E at an altitude of 2877 m). On this platform, various in situ and remote sensing instruments continuously measure the atmospheric dynamics, surface energy balance, radiation, chemistry, aerosol and electricity. Here, we use only meteorological observations at the CRA site which is a rural site located on a plateau in the foothills of the Pyrenees. At the CRA site, standard meteorological observations have been collected since 1995. More details on the P2OA observatory can be found on the website http://p2oa.aero.obs-mip.fr/.

Given the geographical position of the three observatories, various local processes, such as urban heat islands, cloud cover, and mountain/plain breeze circulations, snow cover, and cloud have a role to play concerning daily temperature anomalies.

b. Data used

In order to base our analysis on a common period and on homogeneous data, data from the Meteo-France standard weather station hosted by one CRA-P2OA of three observatories were used for this study. We employed hourly values concerning temperature and incoming shortwave radiation at 2 m, wind speed and direction at 10 m and rainfall between 2003 and 2013. In the framework of the current study, a similar quality control, homogenization and a combination of variables from various sources as seen in the SIRTA-ReOBS were performed for the meteorological variables collected in the Cézeaux-COPDD and CRA-P2OA observatories.

To characterize the influence of large-scale circulations, we based our study mainly on daily temperature anomalies at 2 m above the surface at the three observatories. To ensure that our anomaly was not affected by seasonal variability in temperatures, it was defined by comparison to the average of the current month. We defined the daily temperature anomalies ($aT(j)$) for the day j by removing the 2003-2013 monthly mean temperature at each observatory. This can be expressed through the following equation:

$$aT(j) = < T >_j - < T >_{[m,2003-2013]} \quad (1)$$

where $< T >_j$ is the daily mean temperature for the day j, computed from the mean of hourly temperatures. $< T >_{[m,2003-2013]}$ is the monthly mean temperature calculated over the entire period, and m is the month represented numerically. For example, that $< T >_{[1,2003-2013]}$ was the temperature averaged over all the days in January across the period 2003-2013.

c. Large scale analysis diagnostics

1) WEATHER REGIMES

Weather regimes enable us to describe large-scale atmospheric circulations in a simple manner. With this in mind, we used the classification of weather regimes used by Yiou and Nogaj (2004) and based on the daily anomalies of sea level pressure (SLP) acquired from the NCEP (National Center for Environmental Prediction) reanalyses ($2.5^\circ \times 2.5^\circ$) (Kalnay 1996). The weather regimes are defined in the Euro-Atlantic region (80°W-30°E, 30-70°N) (Fig. 1b, (the larger black square one) and determined from the "K-means" algorithm, itself computed from the first 10 Empirical Orthogonal Functions (EOFs) of seasonal SLP anomalies (Cheng and Wallace 1993; Michelangeli et al. 1995) from 1948 to 2014. The classification used in this study therefore depends on the season. Figure 2 gives an illustration of the four weather regimes defined in winter and their occurrence during the 1948-2014 period. We note in this Figure, the positive (reg. 3) and negative (reg. 4) phases of the North Atlantic Oscillation (respectively NAO^+ and NAO^-), a "Scandinavian blocking" (reg. 2), and the "Atlantic Ridge" (reg. 1). Weather regimes appear with a similar frequency with a 27% occurrence for NAO^+ and "Scandinavian blocking". During the transitional seasons of spring and autumn, a classification into weather regimes is not always appropriate due to seasonal shifts (Vrac et al. 2013). Vrac et al. (2013) found that spring frequently corresponds to an early summer or a longer winter, and that autumn is related to a longer summer or earlier winter, making a definition of a regime during these two seasons difficult. Here, we do not consider this classification for transitional seasons. It is also necessary to consider the stability of the regimes during the winter and summer, as they are sometimes not well defined, and only transitory.

In order to eliminate the days with ambiguous classification in winter and summer, we use a criterion based on the Euclidean distance and the spatial correlation from the nearest weather regime deducted by the K-means method. We filter the classification by eliminating the days for which the Euclidean distance from the nearest weather regime is larger than 10 hPa and with a spatial correlation with the nearest weather regime lower than 0.15. We eliminated 5.2% (52 days) and 10,8% (109 days) of the total days in winter and summer respectively.

Here, we are interested in the influence of the large-scale atmospheric regimes on the variability of daily temperature anomalies (equation 1) in the three observatories. Figure 3 presents the box plot of daily temperature anomalies in winter and summer for each site and for each weather regime during the 2003-2013 period. This Figure shows that in winter, NAO^+ yields relatively milder temperatures at all sites, while NAO^- and blocking are characterized by relatively colder temperatures at all sites. During Atlantic Ridge conditions, the occurrence of either warmer or colder temperatures than those on average is relatively similar, except at SIRTA, where the winter is mostly mild when this regime prevails. It is however, important to note that specific anomalies, warm or cold, can occur whatever the weather regime at SIRTA, whilst very cold winter days are unlikely to occur at Cézeaux-COPDD or CRA-P2OA when NAO^+ or Atlantic Ridge conditions exist. Extreme temperature anomalies are more frequent at SIRTA, and variability is usually enhanced, except during NAO^+. In summer, the weather regimes present almost identically effect on all sites, even if the variability at Cézeaux-COPDD is greater than on the two other sites, and extremes are enhanced. The Atlantic Ridge and NAO^+ have positive daily anomalies on average in winter and summer in all sites, indicating mild and warm temperatures respectively during these two seasons. These results are consistent with those of Yiou et al. (2007) in the fall/winter of 2006/2007. From these results, we can conclude that the weather regimes derived from the

SLP data do not explain the daily temperature anomalies at the three observatories in winter and summer according to the weather regimes derived from the SLP data.

2) LARGE SCALE FLOW ANALOGUES

The slight difference in the anomaly of mean temperatures among the weather regimes in summer, the large variability in the daily temperature anomalies and the fact that the weather regimes are not easily defined in spring and autumn, inspires us to complete the regime approach with the flow analogues method.

The method of atmospheric flow analogues was first introduced by Lorenz (1969). Since then, it has found many applications, including weather prediction (Van den Dool 2007). Yiou et al. (2007) used this approach to infer the connection between surface climate variables and atmospheric circulation. In this study, we use the flow analogue method developed by Yiou et al. (2007) and used by Chiriaco et al. (2014) and Cattiaux et al. (2010) to study climate variability across Europe. For each day during the eleven year period (2003-2013), we looked for days within the same time series which had similar large-scale atmospheric conditions. For this, we considered field anomalies of geopotential height at 500 hPa from the ERA-Interim (ERAI) reanalyses ($0.75^\circ \times 0.75^\circ$) of ECMWF (Dee et al. 2011), a typical diagnostic tool for large-scale circulations. Analogue days were found by minimizing an euclidean distance and maximizing a Spearmann correlation. More details on the flow analogues method can be found in Yiou et al. (2007).

By using the flow-analogues to quantify the relative influence of the large and of the local and mesoscale processes on surface temperature anomalies, we considered two nested domains. The first domain covers the Euro-Atlantic region (80°W-30°E, 30°N-70°N) (Fig. 1b, black square). This domain is also the one used by Cattiaux et al. (2010); Vautard and Yiou (2009); Yiou et al. (2007) and Chiriaco et al. (2014) to establish the link between extreme events (cold waves, heat

waves and drought) and large scale conditions over Europe. The second domain covers the area 21°W-30°E, 30-60°N (Fig. 1b, white square). Compared to the larger domain, this smaller domain (mesoscale) gives more weight to the Mediterranean sea influence on synoptic circulations than does the Atlantic Ocean.

For each day in our studied period and for each domain considered, we kept a maximum of ten analogues, which satisfied the following two criteria: (i) the Spearman spatial correlation had to be greater or equal to 0.6, ensuring the quality of the similarity, and (ii) they should not be closer than 6 days from the current day, in order to ensure that the analogues were independent of the target day (assuming a decorrelation time of 3 days before and 5 days after the target day). These criteria eliminated 6,4 % (around 256 days) and 3 % (around 119 days) of days respectively in terms of the large and small domain. The scores are higher in winter, spring and autumn than in summer for both domains. We found 134 and 54 unselected days respectively for the large and small domain in Summer.

d. Analysis protocol

To quantify the contribution of local processes and large scale circulations at each site, we compared the observed temperature anomalies to the temperature anomalies observed during the analogue days. Figure 4 illustrates this approach for the year 2007 with analogues of circulation computed over the small domain. It shows that, for all observatories, the analogues reproduced the observed temperature anomalies quite well, but they also presented great variability between analogues. For certain days, the analogues could not capture the amplitude of the observed anomalies, as can be seen in the example from 17 to 20 January 2007 on all sites, February 2007 at SIRTA and Cézeaux-COPDD, at the end of August 2007 at CRA-P2OA, and at the end of April 2007 at SIRTA. A smaller standard deviation of the ten anomalies of analogous days combined with an

average closer to the temperature anomaly of the day in question means that the large scale explains the anomaly. In our study, we investigated whether this departure from the observed series relative to the envelope defined by the atmospheric conditions on analogue days can be explained by local processes.

Weather regimes were used to describe and better understand the large-scale influence (see indications of the regimes in Fig. 4).

3. Analysis of large scale conditions versus local processes

In order to estimate the influence of the Mediterranean Sea relative to the Atlantic Ocean at the three sites, we first evaluated the ability of the analogues to represent the observed series using the two different domains described above. Afterward, the difference between the observed series and the temperature anomalies of the analogues was quantified by the definition and the use of an anomaly index. Finally, we focused on specific periods during which the difference was larger than 1.5 °C, tried to identify the relevant processes and discussed the relative contribution of large-scale and local processes.

a. Sensitivity to the Mediterranean Sea

Figure 5 presents the correlation between observed anomalies and those deduced from flow analogues in the large and small domains (Fig. 1b) for each site and for each season. All observed daily temperature anomalies for each season are correlated with those of their 10 analogue days. Thus, for each season of each year from 2003 to 2013, we have one correlation coefficient. This Figure points out larger correlation coefficients in the small domain than in the large domain. This is obvious for the two southern observatories whatever the season, whereas higher correlation coefficients across the small domain are observed only in summer and spring for SIRTA. This

shows that SIRTA is more influenced by large-scale air masses coming from the Atlantic than by mesoscale processes induced by orography and the presence of the Mediterranean Sea, which can strongly influence the weather across southern France (e.g Ducrocq et al. (2008)).

We found a large spatio-temporal variability in the correlation coefficients. CRA-P2OA presented on average the lowest correlation coefficients for the two domains (0.52 and 0.35 respectively for the small and large domain) compared to the two other sites (for the small domain, Cézeaux-COPDD and SIRTA had respectively 0.55 and 0.57 and for the large domain, 0.38 and 0.46 respectively). This difference can be due to its proximity to the Pyrenees, where local processes linked with topography exist: for example, local convection or plain-mountain breeze circulations are more frequent in summer. The two cases of very small correlation coefficient with the small domain (shown in Fig. 5a-b-c on the left bottom with green and black colors) were observed in autumn 2011 at each site, during the winter of 2006 at SIRTA, and during the winter of 2008 at CRA-P2OA and Cézeaux-COPDD. The autumn of 2011 was exceptionally warm. It was indeed the second warmest autumn during the period 1948-2011, and after 2006, according to Cattiaux and Yiou (2012). Cattiaux and Yiou (2012) found that the flow analogues underestimated the amplitude of the seasonal temperature anomaly in Europe during this specific season. This suggests that global warming plays an important role by increasing the concentration of greenhouse gases: the advected air mass is warmer, but it can also enhance local feedbacks.

In the following section, we evaluate the flow analogues approach by considering only the smaller domain, in order to quantify the influence of local processes on the climate variability at the three sites.

b. Large scale influence

We have attempted to better quantify the relative contribution of the large scale versus local processes on the amplitude of temperature anomalies. Since the average signal of the analogues has lower fluctuations than the observed series by construction, we introduce I_m, a new index which will allow two normalized observation and analogue series to be compared.

This index I_m, defined for each month m, represents the normalized monthly average anomaly $< aT(j) >_m$ relative to the standard deviation of the 2003-2013 daily anomalies for the given month m. We compute I_m with:

$$I_m = \frac{< aT(j) >_m}{\sqrt{< (aT(j) - < aT(j) >_{[m,2003-2013]})^2 >_m}}, \tag{2}$$

where $< aT(j) >_{[m,2003-2013]}$ is the average anomaly of temperature of the current month m during the period 2003-2013. In other words, the red line in Fig. 4 is averaged monthly and divided by the standard deviation computed from the monthly anomalies for the period 2003-2013. Concerning the analogue signal, the same definition of the index is applied using all observed anomalies in the analogue days.

Figure 6 represents the time series of this index across the period 2003-2013. The flow analogues reproduce the variability of surface temperature anomalies particularly well. The correlation coefficients between I_m for observations and analogues are 0.80 for SIRTA, 0.85 for Cézeaux-COPDD and 0.86 for CRA-P2OA. This means that the large scale actually plays a predominant role in creating the temperature anomaly variability on monthly scales, which is not surprising.

In Fig. 6, one may note the spatio-temporal variability of I_m in the three observatories. The years 2003 and 2011 were the warmest years on every site for the period 2003-2013, whereas the coldest year on every site was that of 2010 with negative I_m for every month.

While the general trend is well captured by I_m for analogue days, the magnitude of certain events is not reproduced. For example, February 2007 was exceptionally warm with I_m larger than 1.7 at SIRTA and Cézeaux-COPDD according to observations. This peak in temperature is not reproduced by flow analogues with an index of around 0.5 (Fig. 6) when using the small domain, and is even negative when using the large domain (not shown). The large anomaly is not observed at CRA-P2OA. The spatial variability of temperature anomalies during this winter and the difference between observed anomalies and analogues allow us to hypothesize that specific synoptic scale features leading to local anomalies are not resolved by the analogue approach alone and that local processes may have played a specific role at each site during this period.

c. Analysis of specific events during winter 2007

We focused on the winter of 2006/2007 in order to further investigate the contribution of large and local scale processes in the spatio-temporal variability of daily temperature anomalies in the observatories. Note that winter 2007 appears to be the warmest of our study period: it was the second warmest winter in France since 1959 according to climatology established by Meteo-France.

Figure 7 shows the time series of daily temperature anomalies for the winter of 2006/2007 from observations and analogues. It thus corresponds to a zoom of Fig. 4 in January and February 2007. During this period, two regimes, "NAO+" and "Atlantic ridge" are persistent. "NAO^+" is associated with a southwesterly flow over Northern Europe (Michelangeli et al. 1995). We showed in section 2c that the two regimes, "NAO^+" and "Atlantic Ridge" are usually the warmest in winter at all three sites. These results are consistent with those of Yiou et al. (2007) for the exceptionally warm 2006/2007 fall/winter. The regime NAO^- appears between 22 and 26 January, with negative anomalies at all sites. Snow was observed at SIRTA on 23 January, and from 23 to 25 January at CRA-P2OA and Cézeaux-COPDD.

We focused on specific warm events during the winter of 2007 to investigate the role of local processes on the spatio-temporal variability of daily temperature anomalies. We will further analyze two periods /dates: the period 17 to 19 January and a single day: 16 February 2007.

1) 17-19 JANUARY 2007 CASE

The period from 17 to 19 January houses the warmest anomalies of the month of January 2007 at all sites (Fig. 7) with spatial variability in the amplitude: the southern site (CRA-P2OA) presents the lowest daily temperature anomalies compared to the two other sites (warmest anomaly of 9.4, 10 and 7.2 $^{\circ}C$ at SIRTA, Cézeaux-COPDD and CRA-P2OA respectively, on 18 January 2007). The observed positive temperature anomalies are higher than those of analogue days for the whole 17-19 January period at SIRTA and Cézeaux-COPDD and only at CRA-P2OA for the 18 January. Despite the spatial variability in the temperature anomalies, 18 January 2007 presents an anomaly on a large-scale and one can wonder why the anomaly's amplitude of such a large-scale event is not reproduced by any of the analogue days.

To answer this question, the large-scale meteorological situation of analogue days is verified using satellites and ERAI reanalyses and local effects are analyzed based on the meteorological history of the surface measurements and radiosoundings. The meteorological history provides a view of the atmospheric conditions of previous days on a local scale. We consider therefore the diurnal cycles on 18 January 2007 and on the two previous days (16 and 17 January 2007) to point out the effect of the ''local meteorological history'' at each site. Similarly, the ''local meteorological history'' of the five best analogue days on the 18 January 2007 is presented. For example, if the 20 December 2011 is one analogue day for the 18 January 2007, the time series from 18 to 20 December 2011 are displayed.

The large-scale circulation is the NAO^+ regime on the 17 and 18 January, and ''Atlantic ridge'' on 19 January (Fig. 7). Figure 8 presents the wind speed and direction at 600 hPa from the ERAI reanalyses. It shows an increasing westerly wind over France during the 16-18 January period. The five most accurate analogues are generally coherent with an increasing wind speed from 17 to 18 January and show similar wind directions. However, wind speed varies from one analogue to another.

The reflectance in the visible channel at 0.6 μm of MeteoSat Second Generation (MSG) at 1300 UTC on 18 January 2007 is shown in Fig. 9a. Large cloud cover over the North Atlantic and Europe was observed with a window of clear sky over the Mediterranean basin, the South of Spain and the Pyrenees region. Similar cloud cover was also observed on 17 and 19 January 2007 (not shown). The method of Wang and Rossow (1995) was applied to the vertical profile of relative humidity from the radiosoundings at Trappes on 18 January (Fig. 9b) to define the cloud base height. Wang and Rossow (1995) used among other criteria, 87% and 84% as maximum and minimum relative humidity thresholds respectively and relative humidity jumps exceeding 3% at cloud-layer top and base to characterize a cloud-layer. With this method, we find in Fig. 9b that on the 18 January, cloud cover was dominated by low-level clouds with a base not exceeding 700 m in height at 1100 UTC. At 2300 UTC, cloud cover descended and thickened. Based on the Meteo-France weather service station, drizzle was observed that night, with 0.8 mm falling at this site. Combining the satellite image and vertical profiles of relative humidity, we find that these low clouds are stratocumulus clouds associated with the stable atmospheric conditions in the South of Europe linked to the NAO^+ regime. Indeed, the stratocumulus clouds occur widely over Europe in January, according to Hahn and Warren (2007). A similar analysis of the vertical profile of relative humidity for the five most accurate analogue days (Fig. 9b) shows that the 18 January 2007 was the cloudiest day: either there was no cloud cover (analogue day number 3), or there was cloud

cover which disappeared between 1100 and 2300 UTC (analogue day number 1), or much thinner cloud cover (analogue days number 4 and 5). We can expect an effect due to this cloud layer on the 18 January since it impacts the radiative budget at the surface at SIRTA and Cézeaux-COPDD.

The meteorological history of the 18 January and its five most precise analogue days was analyzed with surface measurements. The large scale cloud cover, discussed previously (Fig. 9) impacts incoming solar radiation (ISR) (Fig. 10). The ISR measured at the surface increases from north to south, with very cloudy conditions at SIRTA for every day and almost no reduction of ISR at CRA-P2OA. The integration of ISR across the three days defining the meteorological history period (not shown) demonstrates that there is an obvious lack of ISR for the observed days compared to the analogue days at SIRTA and Cézeaux-COPDD, contrary to CRA-P2OA.

Figure 10 presents the time series of temperature, incoming shortwave radiation at 2 m, wind speed and direction at 10 m above the ground. Cloud cover also clearly impacts the diurnal cycle of 2m-temperature (Fig. 10); Low cloud cover at SIRTA reduces the cooling of the earth and smooths the diurnal temperature cycle. This is also the case at Cézeaux-COPDD, on 18 January. On the contrary, a large diurnal temperature cycle can be observed at CRA-P2OA on most of the days, especially during the period 16-18 January.

At SIRTA, the westerly wind direction at the surface is consistent with the synoptic wind (Fig. 8). The wind direction at Cézeaux-COPDD is very variable but maintains a westerly direction on average, whereas a clear effect of the mountain range can be observed on 16, 17 and some of 18 January at CRA-P2OA, with some slope winds with a north-eastern direction during the day and a southern direction during the night, a sign of the plain-mountain diurnal circulation. Figure 10 shows the diversity of the conditions observed during the analogue days at CRA-P2OA, which makes the comparison difficult. Among the five most accurate analogue days, only three are cloud-free. All of them present a reversal of the wind direction twice a day. This is characteristic of the

slope wind, which seems to play an important role and blurs the comparison of the diurnal cycle. During winter, a lack of cloud cover may allow weak convection over mountains, and certainly greater radiative cooling at night. This southerly mountain breeze during the night advects cool air from the mountains and is associated with low temperatures at night in the diurnal cycle. The mountain breeze which occurs during the NAO^+ regime could then reduce the positive temperature anomaly tendency associated with this regime. The meteorological history of 18 January shows a slope wind regime until noon, when a clear westerly wind settles at the surface. From that moment, the temperature clearly increases, and remains high during the night, with no mountain breezes, between 18 and 19 January. The daily mean temperature then leads to a larger positive temperature anomaly compared with the analogue days with slope winds lasting all day.

From these large and local scales analyses of the observed days and their analogue days, we can ascribe this positive temperature anomaly to a large-scale event observed on the three sites. The NAO^+ regime, which advects mild temperatures from the Atlantic ocean, is characterized by the warmest temperature anomaly in winter (Fig. 3). The flow analogue method shows some limitations however representing this event. The cloud layer is particularly low and deep, and lasts for three days over the northern part of France, whereas nothing in the meteorological history of the analogue days presents such conditions. This cloud cover could imply a warming radiative effect over SIRTA and Cézeaux-COPDD during the 17-19 January period, which would amplify the positive anomaly due to what is already mild air advection. While the low cloud cover observed during this event is not a local effect, its radiative interaction with the surface is dependent on surface temperature and can be considered as a local effect.

In conclusion, it seems that this abnormal warm event stands out from the analogue days, for various reasons- at SIRTA and Cézeaux-COPDD in the first instance and then at CRA-P2OA. The large-scale positive anomaly associated with the NAO^+ regime is amplified at SIRTA and

Cézeaux-COPDD by the warming radiative effect of an unusually low cloud cover occurring over the two sites during the 11 year period. This event, lasting for three days, lead to warmer anomalies than on analogue days. Meanwhile, in CRA-P2OA, the absence of clouds lead to a down-valley wind regime which tends to cool the air at night and to reduce the NAO^+ regime warm anomaly. The down-valley wind was observed on 18 January until midday and did not occur the following night. This lead to higher nocturnal temperatures and warmer daily temperature anomalies than on analogue days the following night. These results show that radiation and cloud cover are important predictors of daily temperature anomalies in winter at this observatory.

2) 16 February 2007 case

16 February 2007 is an example of a case where the temperature anomaly largely exceeded the range of the flow analogues at a single site. A strong and warm anomaly of 12.3 °C was observed at CRA-P2OA on that day, while all analogues showed an anomaly below 8 °C (Fig. 7). At the two other observatories, the temperature anomaly on this day lay within the envelope of the analogues.

The synoptic atmospheric conditions on 16 February were forced by the presence of very low pressure centered over Iceland, and its associated thalweg extending from the island towards the south, near Spain and Morocco. This situation, which often announces the arrival of a front, generated a south-southwesterly wind regime in altitude, bringing dry and warm air from the south. The wind at 600 hPa across the three sites and deduced from the reanalyses of the European Center is shown in Fig. 11 for 16 February and for its analogous days. The analogues have the same types of southwesterly wind regime across the three sites. This situation generally leads to a positive temperature anomaly due to the southern origin of the air mass in many such cases. For this reason, on average, the envelope of the analogues shows a positive temperature anomaly at all sites (Fig. 7).

Southerly winds over the ridge of the Pyrenees correspond to the typical situation of the so-called foehn phenomenon: the East-West orientated mountain ridge is an obstacle for the flow, which can be partially blocked in the lower layers and which can bypass the ridge, with the flow splitting at its sides, or/and passing over and through it across the mountain passes (Scorer 1949, 1953, 1955; Scorer and Klieforth 1959; Seibert 1990; Ólafsson and Bougeault 1997; Jiang et al. 2005). The adiabatic descent of air in the lee, usually occurring together with the flow over the mountain, is associated with a typical drying and warming in the lower lee air layers on the French side ('foehn effect').

One of the most important governing variables for this phenomenon is the upwind wind profile, and particularly the upwind component, which is perpendicular to the ridge: the larger this component, the easier it is for the flow to go over the mountain and generate the foehn effect (Seibert 1990). For the Pyrenees in the vicinity of the CRA-P2OA site, we evaluate the cross-component at 210° azimuth (± 10°): that is, a wind with this direction (which is very similar to a southerly wind) travels exactly transversely to the ridge, on a 150 km horizontal scale. This direction is also aligned with the main Aure Valley, which is situated south of the CRA-P2OA observatory and North-South orientated. Figure 12a shows the upwind profiles of the cross-ridge component (projection of the wind on the 210° axis), for 16 February and for all analogues, at 0000 UTC. These are deduced from the radiosoundings launched daily from Zaragosa in Spain, which is located about 150 km south of the ridge of the Pyrenees, and 200 km from the CRA-P2OA site. These profiles confirm the potential to generate the foehn effect at CRA-P2OA for most of the days shown, as this component is positive for most cases above 1000 m. It also reveals that 16 February is the case with the strongest 210° upwind component between 1000 m and 6000 m, especially below 3500 m, making it the most favorable case for a strong foehn event (the highest peak in the

Pyrenees is at 3400 m). Figure 11 also shows that the upwind wind increased significantly during the day.

Figure 12b presents the visible image of MSG at 1500 UTC on 16 February 2007. This day was marked by large cloud cover over the western Atlantic and northern Europe, and a clear sky above the Mediterranean basin and eastern Europe. Cloud cover over the Pyrenees shows that the sky was clear in Spain and in the lee of the mountain (where CRA-P2OA is situated). Further to the north, a cloud with a well-defined southern border, typical of the upward branch of a mountain wave, can be observed, and is usually associated with foehn and southerly overpassing flows. The clear sky in Spain reveals a ‘‘dry foehn’’ as opposed to some cases, where clouds are blocked on the Spanish side, with some rain that can contribute to the drying and warming effect of the air in the lee on the French side. This means that on 16 February, air mass was generally very dry on the large-scale, a fact which is confirmed by the radiosoundings of Zaragosa, Bordeaux (Atlantic French coast), Trappes (close to Paris), and the synoptic situation discussed before. The soundings of Trappes at 1100 and 2300 UTC show very dry and warm air between 800 m and 4000 m. Above this altitude, fine medium clouds (of about 500 m) are observed (not shown).

We can now consider the observations at the surface of the different observatories. Figure 13 presents the evolution of the meteorological variables observed close to the surface on 16 February 2007, and of its analogues. The most striking feature is found in the surface wind at CRA-P2OA: for all the analogues, the wind at the surface is southerly during the night and northerly during the day. This, along with the low associated wind speed (below 6 m s^{-1}), is the influence of the mountain-plain diurnal circulation. That is to say, although the upwind flow is from the south, and sometimes has a strong wind speed (Fig. 12a), this does not prevent the plain-mountain circulation from settling during those analogue days. It is actually quite classic, with the southerly wind kept at a higher level. Note that this does not prevent the foehn effect (warming and drying in the

lee), or the warmer local temperature that can be found at this site relative to the other sites. On 16 February, however, the wind at the surface of CRA-P2OA remained southerly all day, with the wind speed increasing during the day, by up to 10 m s^{-1} at times. This means that for this specific day, the upwind flow was strong enough to be able to create a downslope wind throughout the entire day in which case, the warming and drying effect in the lee is still larger. This is consistent with Fig. 12a, which shows the singularity of this day in terms of upwind conditions. It probably explains most of the temperature anomalies found at CRA-P2OA, which exceed the usual anomalies found in analogous synoptic situations (Fig. 7).

At Cézeaux-COPDD, this synoptic situation does not lead to a marked anomaly, but the general dry and warm air leads to a large diurnal increase. The night of 16 to 17 February may have been influenced by a small foehn effect, in the presence of westerly winds (typically occurring in the ''Chaine des puys'' mountains to the west of the site). The air temperature does not decrease much, and the wind continues to arrive from the west. At SIRTA, the wind at the surface is easterly, surprisingly, while the sounding at Trappes shows a strong southerly flow down to the lowest levels of the atmosphere. This weak easterly wind at SIRTA seems unconnected to the warm, dry southerly air above, and could explain the relative lower temperature found on 16 February (relative to its analogues).

This event shows how sub-mesoscale processes linked with orography can amplify a temperature anomaly which is first of all forced at the synoptic scale. This specific type of amplification has been previously observed by Takane and Kusaka (2011) in Japan in the summer.

4. Summary and Conclusions

This study aimed to evaluate the relative contribution of large scale atmospheric circulation and more local processes to daily temperature anomalies over a North-South transect of France. The

study was based on the observations of meteorological variables on three observatories and on NCEP and ECMWF reanalyses. The flow analogues methods was used in particular to diagnose the fingerprint of the large scale synoptic circulation concerning the temperature anomaly, and to highlight the potential role of local processes in inhibiting or amplifying the anomaly.

The analysis of weather regimes over the Euro-Atlantic region shows that the large-scale atmospheric circulations have an important influence on the daily temperature anomalies at the three observatories in winter. The "NAO^{+}" and "Atlantic Ridge" appear to be the warmest regimes in this season. While the influence of the four weather regimes on daily temperature anomalies does not statistically differ at the three observatories in the summer due to strong variability within each regime, extreme anomalies are associated with one or two regimes at all observatories except for that of SIRTA.

The approach of flow analogues over two different domains shows that SIRTA is less affected by the mesoscale processes formed around the Mediterranean Sea than are the two other observatories, which is not surprising considering its northern location.

The atmospheric circulation analogue method demonstrates the large correlation between a monthly temperature anomaly index calculated from the observed series and that which is provided by the representation of the analogues. This highlights the predominant role played by the large-scale situation in the temperature anomalies. Sometimes, however, the amplitude of the monthly temperature index is not captured by the flow analogues and presents a large spatial variability between the three observatories. It is suggested that these discrepancies are related to local processes. Two specific events revealed in the warmest winter in the period 2003-2013 are further analyzed to test this hypothesis: 1/ the 17-19 January 2007 event which had the strongest positive temperature anomaly at the two northern observatories (SIRTA and Cézeaux-COPDD) and,

2/ the 16 February 2007, for which only CRA-P2OA presented a very large positive temperature anomaly, found beyond the signal of the set of analogues.

From the analysis of these two events, the impact of several local processes have been identified:

1/ the local impact of non-local cloud cover during westerly wind conditions in winter: low-level clouds have been shown to increase the positive temperature anomaly at SIRTA and Cézeaux-COPDD in these conditions, partly due to the positive radiative green-house effect of the clouds.

2/ the orographic impact: CRA-P2OA and Cézeaux-COPDD are both in proximity to mountains and are frequently impacted by either the foehn or slope wind effect. In a weak large-scale situation, the slope breeze easily settles at CRA-P2OA, and can transport cool air from the mountain during the night in winter. Foehn events observed at both the CRA-P2OA and Cézeaux-COPDD sites with southerly and westerly wind conditions respectively, can amplify positive temperature anomalies, originally forced by the large scale.

The analysis of two specific events reveals that some local processes are able to modulate the trend of the daily temperature anomaly driven by the large-scale atmospheric circulation. However, such a phenomenological approach remains difficult, since the understanding of one event necessitates the analysis of the meteorological history of not only the event itself, but also of its analogue days. To investigate the impact of local processes, a systematic study of all cases in which observations differ from analogue days would be necessary.

Departures between observed local anomalies and analogues might not only be due to local processes but also to differences between the observed event and its analogues on the synoptic scale, which would not be adequately resolved by the classical analogue approach employed. A possibility for the investigation of this is the combining of different variables in the analogues method (vorticity, water vapor, temperature, wind), even if this would require much longer series in order to ensure a large enough number of analogues for each day.

Acknowledgments. This work was carried out in the context of ROSEA, and funded by ALLENVI. The ROSEA program now belongs to a larger program and national network called ATMOS (Atmospheric Short-Lived Climate Forcers Observing System). The administrative and technical supervision of the observatories have been acknowledged. Part of the data used here were collected at the Pyrenean Platform for Observation of the Atmosphere P2OA, Observatoire de Physique du Globe de Clermont Ferrand OPGC and Site Instrumental de Recherche par Télédétection Atmosphérique SIRTA. P2OA facilities and staff were funded and supported by the Observatoire Midi-Pyrénées (University of Toulouse, France) and the CNRS (Centre National de la Recherche Scientifique) INSU (Institut National des Sciences de l'Univers). OPGC facilities and staff were funded and supported by the Blaise Pascal University of Clermont Ferrand and CNRS (Centre National de la Recherche Scientifique) INSU. We are grateful to NCEP, ECMWF, and Meteo-France for providing the observation data and global model reanalyses used in this study. We acknowledge the CNES for partially funding M. Chiriaco's research. P. Yiou was supported by an ERC advanced grant (No. 338965 - A2C2). The authors would like to thank the three anonymous reviewers for their fruitful comments, which helped us to improve the manuscript. Finally, we thank Naomi Rivière for carefully proof reading our manuscript.

References

Bastin, S., M. Chiriaco, and P. Drobinski, 2016: Control of radiation and evaporation on temperature variability in a wrf regional climate simulation: comparison with colocated long term ground based observations near paris. *Climate Dyn.*, doi:10.1007/s00382-016-2974-1.

Boé, J., and L. J. Terray, 2014: Land-sea contrast, soil-atmosphere interactions and cloud-temperature interactions: interplays and roles in future summer european climate change. *Climate Dyn.*, **42(3-4)**, 683–699.

Cassou, C., L. Terray, and A. S. Phillips, 2005: Tropical atlantic influence on european heat waves. *J. Climate*, **18**, 2805–2811.

Cattiaux, J., R. Vautard, C. Cassou, P. Yiou, V. Masson-Delmotte, and F. Codron, 2010: Winter 2010 in europe: A cold extreme in a warming climate. *Geophys. Res. Lett.*, **37**, doi:10.1029/2010GL044613.

Cattiaux, J., and P. Yiou, 2012: Contribution of atmospheric circulation to remarkable European temperatures of 2011, in Explaining Extreme Events of 2011 from a Climate perspective . *Bull. Amer. Meteor. Soc.*, **93**, 1041–1067, doi:10.1175/BAMSD-12-00021.1.

Cheng, X. H., and J. M. Wallace, 1993: Cluster analysis of the northern hemisphere wintertime 50 hpa height field: Spatial patterns. *J. Atmos. Sci.*, **50(16)**, 2674–2696.

Cheruy, F., J. L. Dufresne, F. Hourdin, and A. Ducharne, 2014: Role of clouds and land-atmosphere coupling in midlatitude continental summer warm biases and climate change amplification in cmip5 simulations. *Geophys. Res. Lett.*, **41**, 6493–6500.

Cheruy, F., J. C. Dupont, A. Campoy, A. Ducharne, F. Hourdin, M. Haeffelin, and M. Chiriaco, 2013: Combined influence of atmospheric physics and soil hydrology on the realism of the lmdz model compared to sirta measurements. *Climate Dyn.*, **40**, 2251–2269, doi:10.1007/s00382-012-1469-y.

Chiriaco, M., S. Bastin, P. Yiou, M. Haeffelin, J. C. Dupont, and M. Stéfanon, 2014: European heatwave in july 2006: Observations and modeling showing how local processes amplity cinducive large-scale conditions. *Geophys. Res. Lett.*, **41**, doi:10.1002/2014GL060205.

Dee, D. P., and Coauthors, 2011: The era-interim reanalysis: configuration and performance of the data assimilation system. *Quart. J. Roy. Meteor. Soc.*, **137**, 553–597, doi:DOI:10.1002/qj.828.

Ducrocq, V., O. Nuissier, D. Ricard, C. Lebeaupin, and T. Thouvenin, 2008: A numerical study of three catastrophic precipitating events over southern france. part ii: Mesoscale triggering and stationarity factors. *Quart. J. Roy. Meteor. Soc.*, **134**, 131–145.

Fischer, E. M., S. I. Seneviratne, D. Lüthi, and C. Schär, 2007b: The contribution of land-atmosphere coupling to recent european summer heatwaves. *Geophys. Res. Lett.*, **34**, L06707, doi:10.1029/2006GL029068.

Haeffelin, e. a., M., 2005: Sirta, a ground-based atmospheric observatory for cloud and aerosol research. *Ann. Geophys.*, **23**, 253–275.

Hahn, C. J., and S. G. Warren, 2007: A gridded climatology of clouds over land (1971-96) and ocean (1954-97) from surface observations worldwide. Numeric data package ndp-026e ornl/cdiac-153, cdiac, Department of Energy. doi:10.3334/CDIAC/cli.ndp026e.

Jiang, Q., J. D. Doyle, and R. B. Smith, 2005: Blocking, descent and gravity waves: Observations and modeling of a map northerly föhn event. *Quart. J. Roy. Meteor. Soc.*, **131**, 675–701.

Kalnay, e. a., E., 1996: The ncep/ncar 40-year reanalysis project. *Bull. Amer. Meteor. Soc.*, **77**, 437–471.

Lorenz, E. N., 1969: Atmospheric predictability as revealed by naturally occurring analogues. *J. Atmos. Sci.*, **26**, 636–646.

Luterbacher, J., and Coauthors, 2007: Exceptional european warmth of autumn 2006 and winter 2007: Historical context, the underlying dynamics, and its phenological impacts. *Geophys. Res. Lett.*, **34**, L12704, doi:10.1029/2007GL029951.

Michelangeli, P. A., R. Vautard, and B. Legras, 1995: Weather regimes: Recurrence and quasi stationarity. *J. Atmos. Sci.*, **52**, 1237–1256.

Miralles, D. G., A. J. Teuling, C. C. V. Heerwaarden, and J. V. G. de Arellano, 2014: Mega-heatwave temperatures due to combined soil desiccation and atmospheric heat accumulation. *Nature Geosci.*, **7**, 345–349.

Ólafsson, H., and P. Bougeault, 1997: The effect of rotation and surface friction on orographic drag. *J. Atmos. Sci.*, **54**, 193–210.

Quesada, B., R. Vautard, P. Yiou, M. Hirschi, , and S. I. Seneviratne, 2012: Asymmetric european summer heat predictability from wet and dry southern winters and springs. *Nature Climate Change.*, **2**, 736–741, doi:10.1038/nclimate1536.

Schär, C., P. L. Vidale, D. Luthi, C. Frei, C. Haberli, M. A. Linigier, and C. Appenzeller, 2004: The role of increasing temperature variability in european summer heatwaves. *Nature*, **427**, 332–336.

Scorer, R. S. I., 1949: Theory of waves in the lee of mountains. *Quart. J. Roy. Meteor. Soc.*, **75**, 41–56.

Scorer, R. S. I., 1953: Theory of mountain waves: Ii - The flow over ridge. *Quart. J. Roy. Meteor. Soc.*, **79**, 70–83.

Scorer, R. S. I., 1955: Theory of mountain waves: Iv - separation of flow from the surface. *Quart. J. Roy. Meteor. Soc.*, **81**, 340–350.

Scorer, R. S. I., and H. Klieforth, 1959: Theory of mountain waves of large amplitude. *Quart. J. Roy. Meteor. Soc.*, **85**, 131–143.

Seibert, P., 1990: South foehn studies since the alpex experiment. *Meteor. Atmos. Phys.*, **43**, 91–103.

Seneviratne, S. I., D. Lüthi, M. Litschi, and C. Schär, 2006: Land-atmosphere coupling and climate change in europe. *Nature*, **443**, 205–209.

Seneviratne, S. I., P. Viterbo, D. Lüthi, and C. Schär, 2004: Inferring changes in terrestrial water storage using era-40 re-analysis data: The mississippi river basin. *J. Climate*, **17**, 2039–2057.

Stefanon, M., P. Drobinski, F. D'Andrea, C. Lebeaupin-Brossier, and S. Bastin, 2014: Soil moisture-temperature feedbacks at meso-scale during summer heat waves over western europe. *Climate Dyn.*, **42(4-5)**, 1309–1324, doi:0.1007/s00382-013-1794-9.

Stegehuis, A. I., A. J. Teuling, P. Ciais, R. Vautard, and M. Jung, 2013: Future european temperature change uncertainties reduced by using land heat flux observations. *Geophys. Res. Lett.*, **40**, 2242–2245, doi:10.1002/grl.50404.

Takane, Y., and H. Kusaka, 2011: Formation mechanisms of the extreme high surface air temperature of 40.9^{o}c observed in the tokyo metropolitan area: Considerations of dynamic foehn and foehnlike wind. *J. Appl. Meteor. Climatol.*, **50**, 1827–1841.

Van den Dool, H., 2007: *Empirical Methods in Short-Term Climate Prediction*. Oxford University press.

Vautard, R., and P. Yiou, 2009: Control of recent european surface climate by atmospheric flow. *Geophys. Res. Lett.*, **36**, L22702, doi:10.1029/2009GL040480.

Vautard, R., and Coauthors, 2007: Summertime european heat and drought waves induced by wintertime mediterranean rainfall deficit. *Geophys. Res. Lett.*, **34**, L07711, doi:10.1029/2006GL028001.

Vrac, M., P. V. Ayar, and A. Yiou, 2013: Trends and variability of seasonal weather regimes. *Int. J. Climatol.*, **34**, 472–480, doi:10.1002/joc.3700.

667 Wang, J. H., and W. B. Rossow, 1995: Determination of cloud structure from upper-air observa-
668 tions. *J. Appl. Meteor.*, **34**, 2243–2258.

669 Yiou, P., K. Goubanova, X. Z. Li, and M. Nogal, 2008: Weather regime dependence of extreme
670 value statistics for summer temperature and precipitation. *Nonlin. Processes. Geophys.*, **15**,
671 365–378, doi:10.5194/npg-15-365-2008.

672 Yiou, P., and M. Nogaj, 2004: Extreme climatic events and weather regimes over the north atlantic:
673 When and where? *Geophys. Res. Lett.*, **31**, L07202, doi:10.1029/2003/GL019119.

674 Yiou, P., R. Vautard, P. Naveau, and C. Cassou, 2007: Inconsistency between atmospheric dy-
675 namics and temperatures during the exceptional 2006/2007 fall/winter and recent warming in
676 europe. *Geophys. Res. Lett.*, **34**, L21808, doi:10.1029/2007GL031981.

677 Zampieri, M., F. D'Andrea, R. Vautard, P. Ciais, N. de Noblet-Ducoudr, and P. Yiou, 2009: Hot
678 european summers and the role of soil moisture in the propagation of the mediterranean drought.
679 *J. Climate*, **22**, 4747–4758.

680 [FIG. 1 about here.]

681 [FIG. 2 about here.]

682 [FIG. 3 about here.]

683 [FIG. 4 about here.]

684 [FIG. 5 about here.]

685 [FIG. 6 about here.]

686 [FIG. 7 about here.]

[FIG. 8 about here.]

[FIG. 9 about here.]

[FIG. 10 about here.]

[FIG. 11 about here.]

[FIG. 12 about here.]

[FIG. 13 about here.]

LIST OF FIGURES

Fig. 1. (a) Orography of France and the locations of the SIRTA, COPDD and P2OA observatories (adapted from http://carthoteque.free.fr). (b) Sea level pressure on 1 January 2003 from NCEP over the Euro-Atlantic domain used to define weather regimes and flow analogues in the large domain. The white square delimits the small domain used in the flow analogues method (see section 2). 36

Fig. 2. Occurrence of North Atlantic weather regimes computed from the SLP from NCEP reanalyses in winter during the period 1948-2014. The frequency of of each regime is in percentages at the top of each picture. Reg. refers to the weather regime and Reg. 1 is "Atlantic Ridge", Reg. 2 is the "blocking", Reg. 3 is NAO^+, and Reg. 4 is NAO^-. The isolines indicate the SLP anomalies in hPa. 37

Fig. 3. Box plots of daily temperature anomalies for each weather regime during the period 2003-2013 at the three sites of the ROSEA network. 38

Fig. 4. Time series of daily temperature anomalies observed in 2007, (red) on current days and (gray) on analogue days at (a-d) SIRTA, (b-e) Cézeaux-COPDD and (c-f) CRA-P2OA. Colored bands at the top of each picture indicate the weather regime observed for each day: (blue) "NAO^+" (black) "NAO^-" (cyan) "Atlantic Ridge" and (red) "Blocking". The gray envelope delimits the extreme values of the daily temperature anomalies from the set of analogue days. "an2" indicates the temperature anomalies of the analogue days computed in the small domain. Vertical blue dashed lines indicate the 17-20 January 2007 period. 39

Fig. 5. Scatter plots of seasonal correlation coefficients between the large and small domain. The correlation coefficients are computed between observed and all analogue day temperature

anomalies. Each color represents one season: winter (December-February) in black, spring (March to May) in blue, summer (June to August) in red and autumn (September to November) in green. The black cross indicates the winter of 2007. 40

Fig. 6. Time series of the monthly normalized index of temperature anomalies observed (red line) and deduced from flow-analogues of the small domain (black line). The vertical dashed lines delimit the four seasons of the year (DJF, MAM, JJA, and SON). 41

Fig. 7. As in Fig. 4, but zoomed in on January-February 2007. Horizontal black segments indicate the two specific events analyzed in sections 3.c.1) and 3.c.2). Colored squares at the top of each picture indicate the weather regime observed for each day: (blue) "NAO^+" (black) "NAO^-" (cyan) "Atlantic Ridge" and (red) "Blocking". 42

Fig. 8. Time series at each site of wind speed and direction for the period from 16 to 18 January 2007 at 600 mb. The observed series are represented in "black" while the other colors represent the five most accurate analogue days for 18 January 2007. 43

Fig. 9. (a) Reflectance in the visible channel of MSG/SEVIRI at 0.6 μm on 18 January 2007 at 1300 UTC. This picture is available on http://www.icare.univ-lille1.fr. Red points in (a) indicate the location of the three observatories. (b) Vertical profile of relative humidity at SIRTA at 1100 and 2300 UTC, respectively, on 18 January 2007. Solid lines indicate the observed vertical profiles, while dashed lines represent the five most accurate analogues. Vertical dashed lines in (b) indicate the minimum (84%) and maximum (87%) relative humidity used by Wang and Rossow (1995) to estimate cloud vertical structure: cloud-top and cloud-base heights. No radiosoundings at 2300 UTC for the analogue days number 2 and 3. 44

Fig. 10. Time series at each site of the temperature, incoming shortwave radiation (ISR), wind speed and direction during the period 16 to 18 January 2007. The observed series are represented in "black", while the other colors represent the historical data of the five most accurate analogue days for 18 January 2007. 45

Fig. 11. As in Fig. 8 but for 16 February. 46

Fig. 12. (a) Reflectance in the visible channel of MSG/SEVIRI at 0.6 μm on 16 February 2007 at 1500 UTC. This picture is available on the following site: http://www.icare.univ-lille1.fr. Red points in (b) indicate the location of the three observatories; the blue point represents the radiosonde station in Zaragosa. (b) Vertical profiles of the wind component transversal to the Pyrenees ridge (210°) observed at Zaragosa, Spain, on 16 February and the entirety of its analogues, at 0000 UTC, ... 47

Fig. 13. As in Fig. 10 but for 16 February. 48

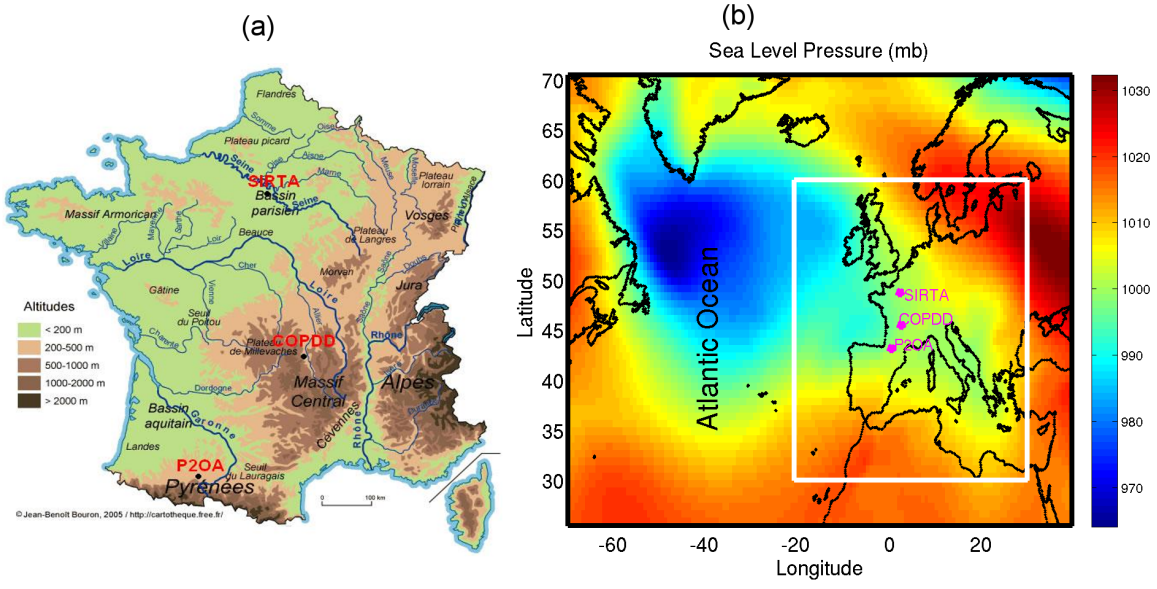

748 FIG. 1. (a) Orography of France and the locations of the SIRTA, COPDD and P2OA observatories (adapted
749 from http://carthoteque.free.fr). (b) Sea level pressure on 1 January 2003 from NCEP over the Euro-Atlantic
750 domain used to define weather regimes and flow analogues in the large domain. The white square delimits the
751 small domain used in the flow analogues method (see section 2).

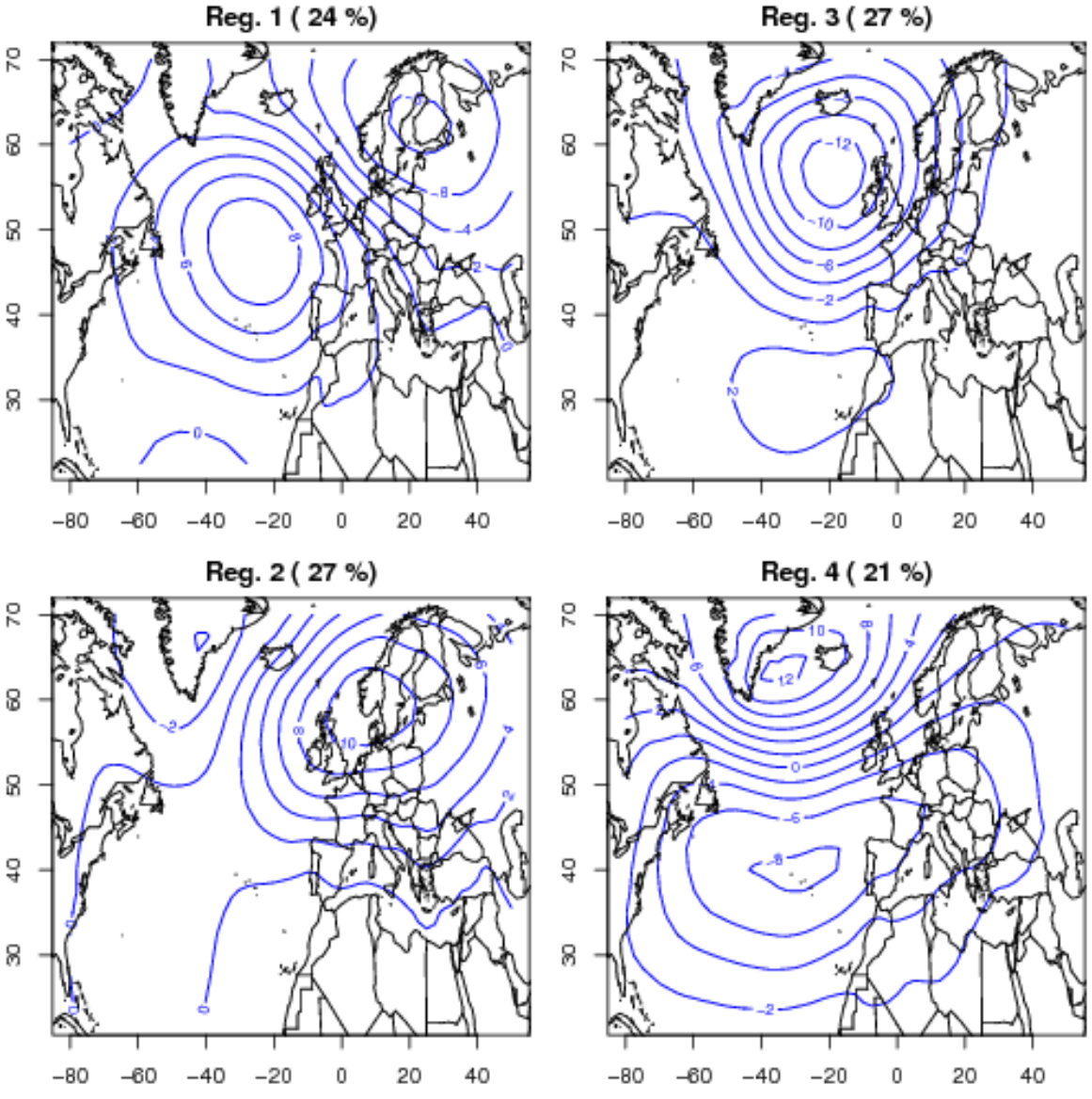

FIG. 2. Occurrence of North Atlantic weather regimes computed from the SLP from NCEP reanalyses in winter during the period 1948-2014. The frequency of of each regime is in percentages at the top of each picture. Reg. refers to the weather regime and Reg. 1 is "Atlantic Ridge", Reg. 2 is the "blocking", Reg. 3 is NAO^+, and Reg. 4 is NAO^-. The isolines indicate the SLP anomalies in hPa.

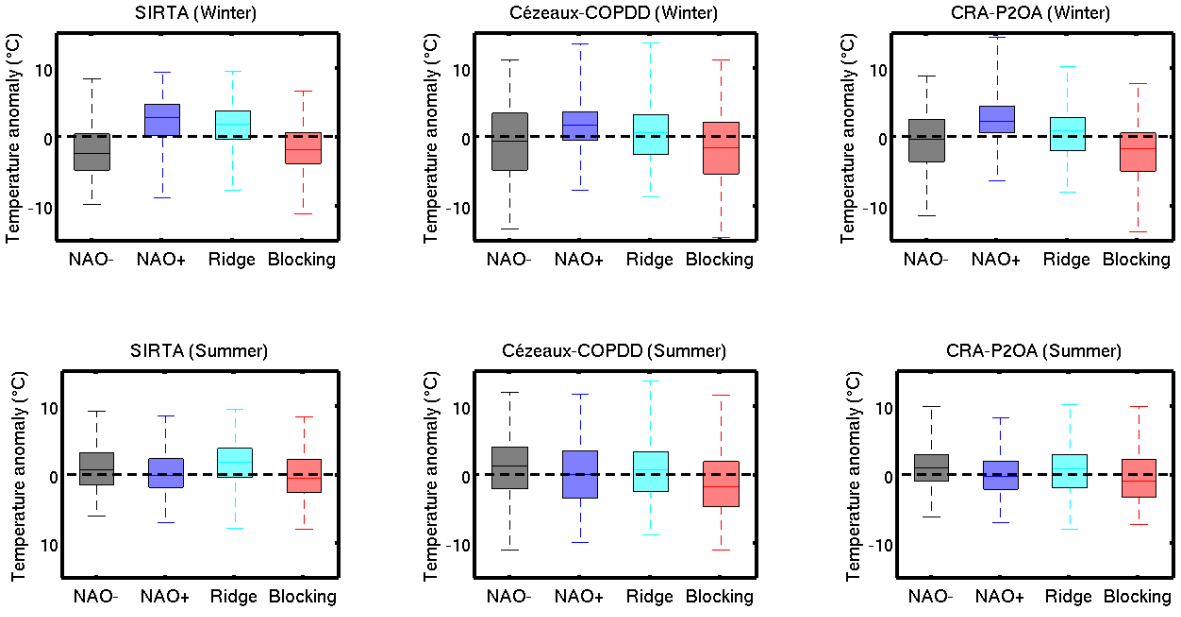

FIG. 3. Box plots of daily temperature anomalies for each weather regime during the period 2003-2013 at the three sites of the ROSEA network.

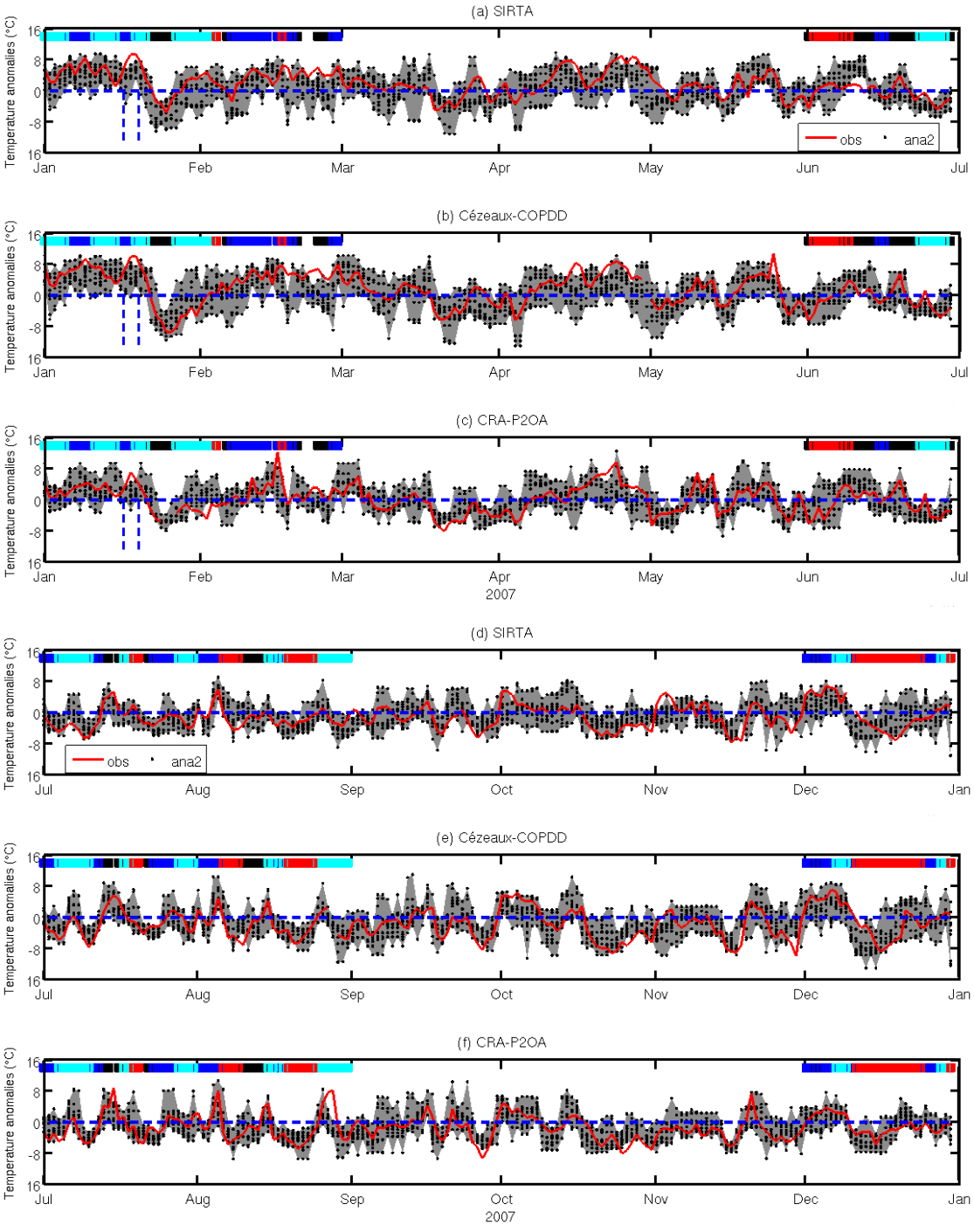

FIG. 4. Time series of daily temperature anomalies observed in 2007, (red) on current days and (gray) on analogue days at (a-d) SIRTA, (b-e) Cézeaux-COPDD and (c-f) CRA-P2OA. Colored bands at the top of each picture indicate the weather regime observed for each day: (blue) "NAO^+" (black) "NAO^-" (cyan) "Atlantic Ridge" and (red) "Blocking". The gray envelope delimits the extreme values of the daily temperature anomalies from the set of analogue days. "an2" indicates the temperature anomalies of the analogue days computed in the small domain. Vertical blue dashed lines indicate the 17-20 January 2007 period.

(a) SIRTA

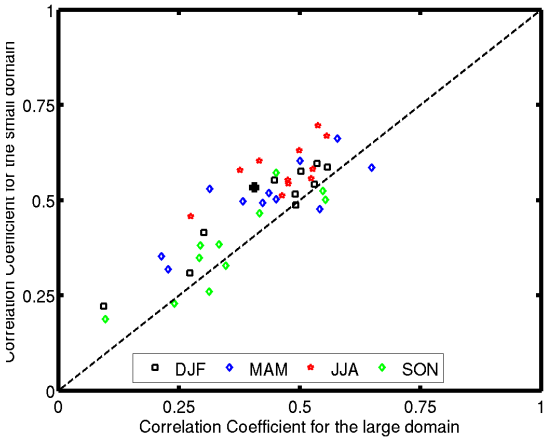

(b) Cézeaux-COPDD

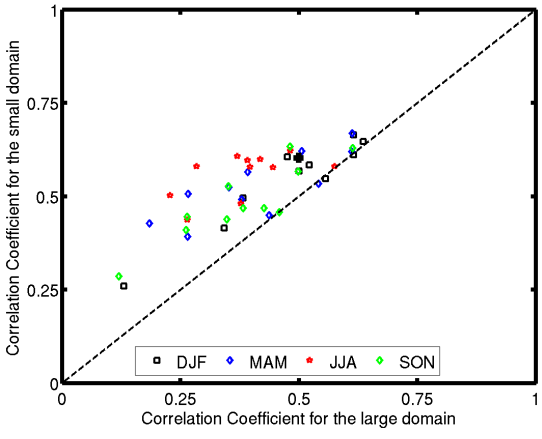

(c) CRA-P2OA

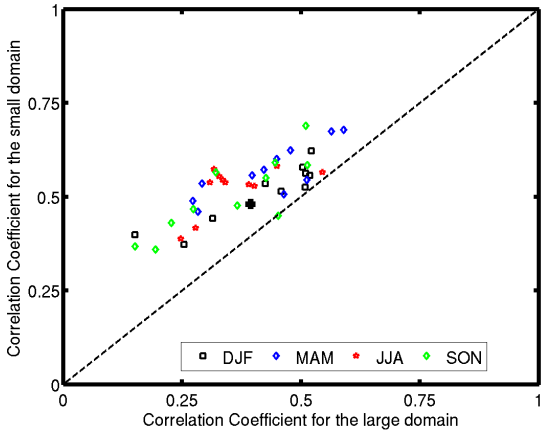

764 FIG. 5. Scatter plots of seasonal correlation coefficients between the large and small domain. The correlation
765 coefficients are computed between observed and all analogue day temperature anomalies. Each color represents
766 one season: winter (December-February) in black, spring (March to May) in blue, summer (June to August) in
767 red and autumn (September to November) in green. The black cross indicates the winter of 2007.

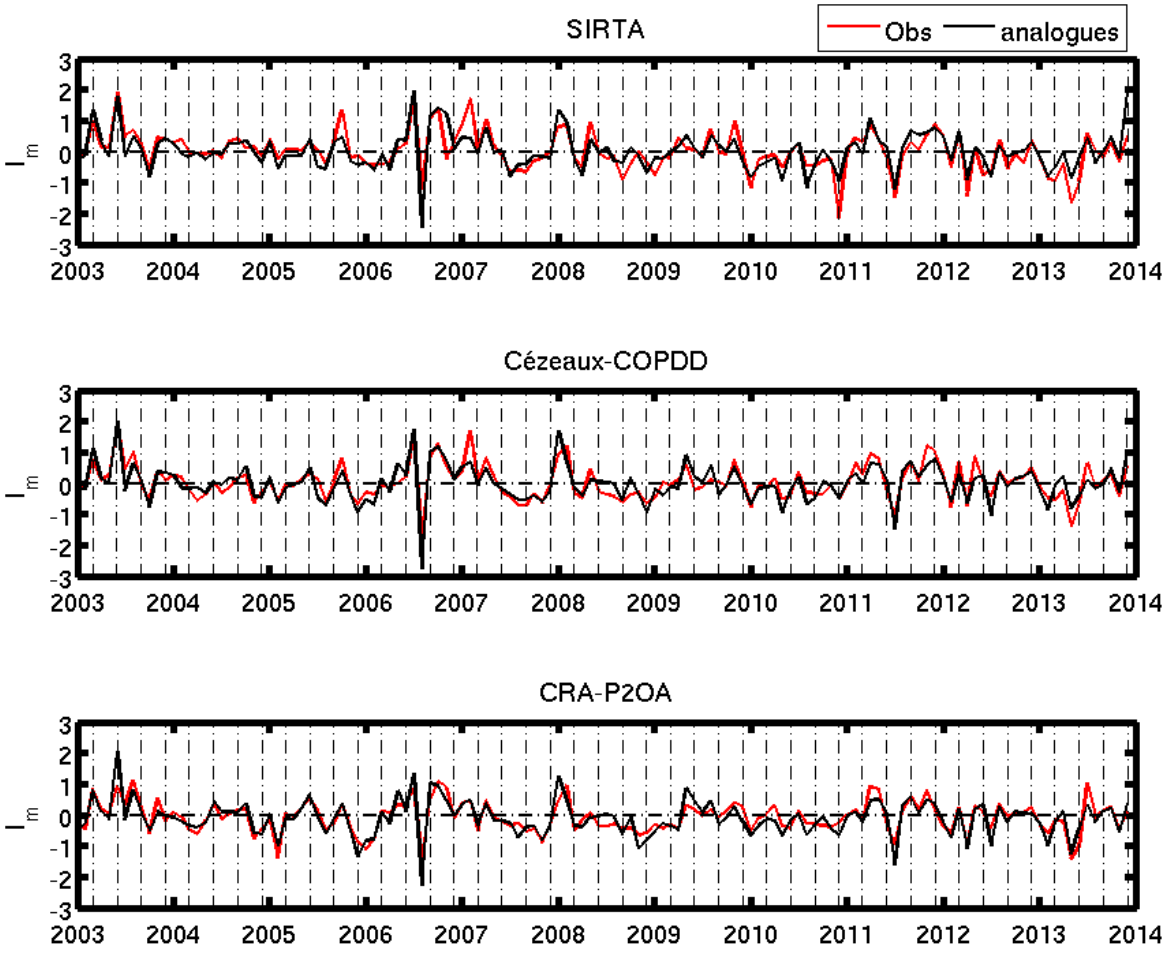

768 FIG. 6. Time series of the monthly normalized index of temperature anomalies observed (red line) and de-
769 duced from flow-analogues of the small domain (black line). The vertical dashed lines delimit the four seasons
770 of the year (DJF, MAM, JJA, and SON).

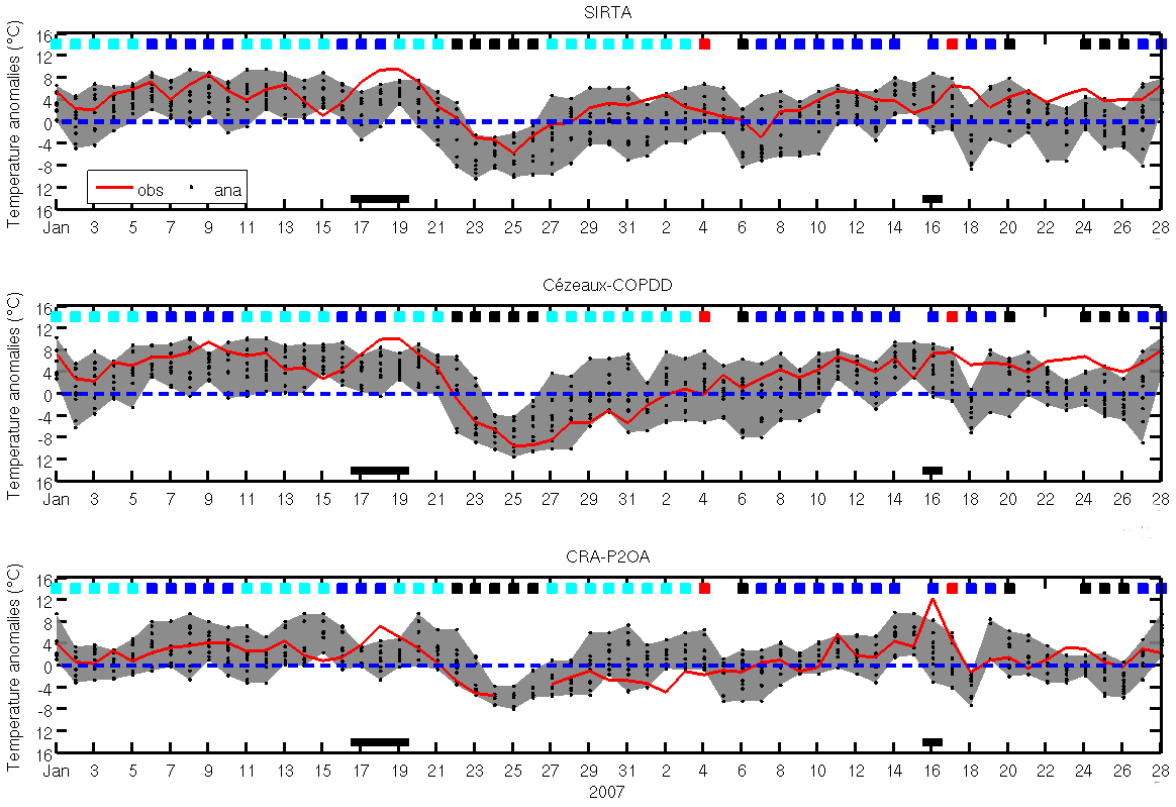

771 FIG. 7. As in Fig. 4, but zoomed in on January-February 2007. Horizontal black segments indicate the two
772 specific events analyzed in sections 3.c.1) and 3.c.2). Colored squares at the top of each picture indicate the
773 weather regime observed for each day: (blue) "NAO^+" (black) "NAO^-" (cyan) "Atlantic Ridge" and (red)
774 "Blocking".

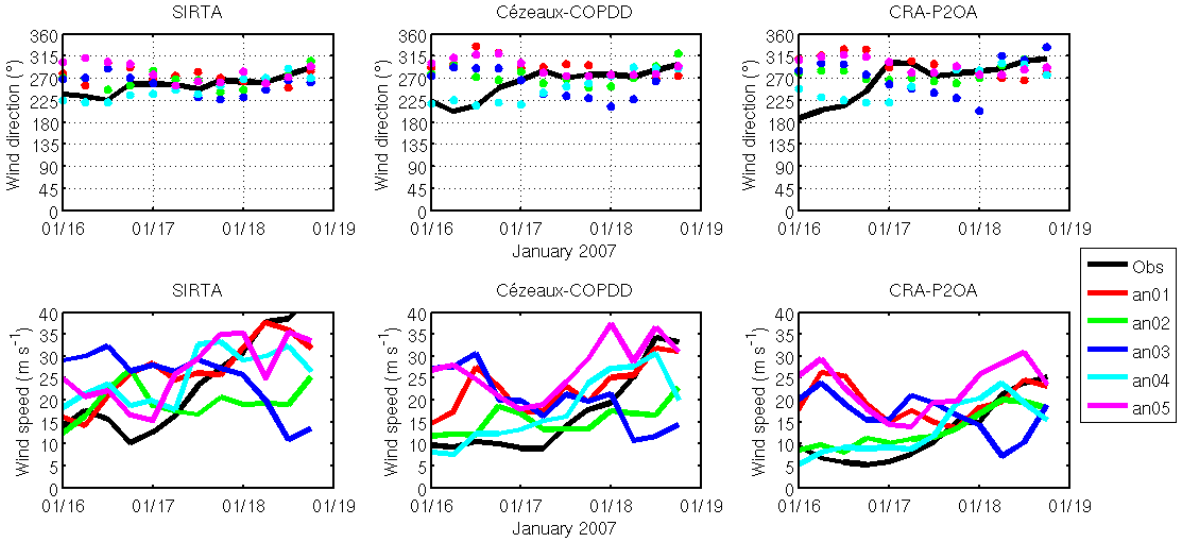

FIG. 8. Time series at each site of wind speed and direction for the period from 16 to 18 January 2007 at 600 mb. The observed series are represented in "black" while the other colors represent the five most accurate analogue days for 18 January 2007.

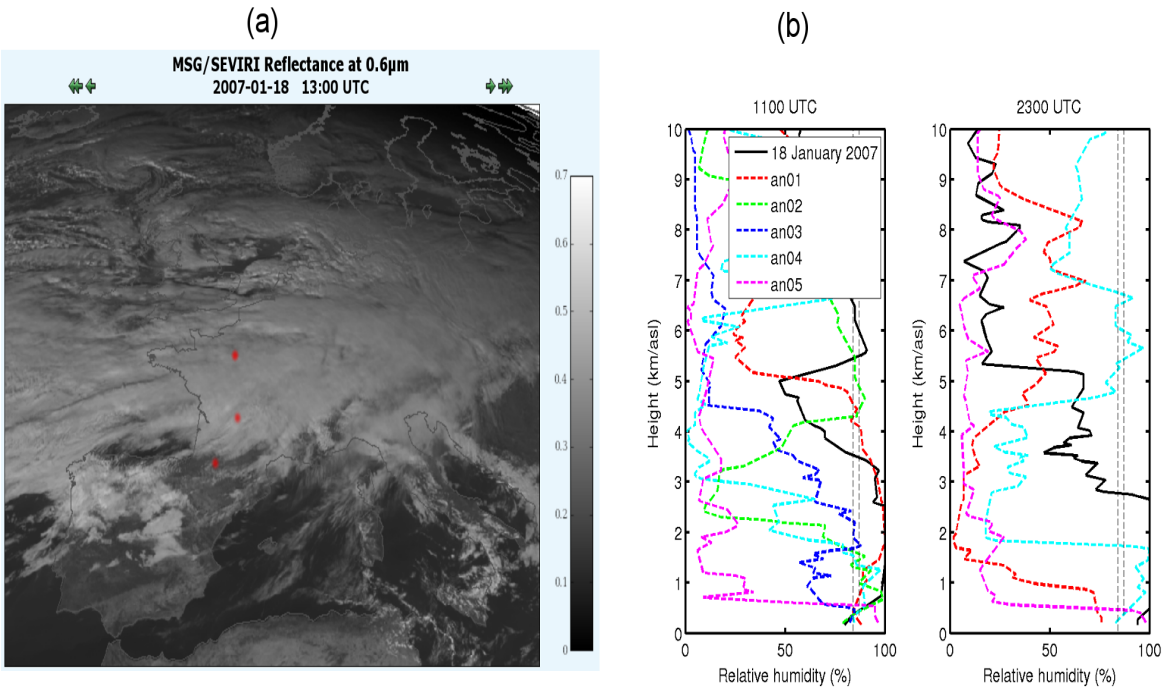

FIG. 9. (a) Reflectance in the visible channel of MSG/SEVIRI at 0.6 μm on 18 January 2007 at 1300 UTC. This picture is available on http://www.icare.univ-lille1.fr. Red points in (a) indicate the location of the three observatories. (b) Vertical profile of relative humidity at SIRTA at 1100 and 2300 UTC, respectively, on 18 January 2007. Solid lines indicate the observed vertical profiles, while dashed lines represent the five most accurate analogues. Vertical dashed lines in (b) indicate the minimum (84%) and maximum (87%) relative humidity used by Wang and Rossow (1995) to estimate cloud vertical structure: cloud-top and cloud-base heights. No radiosoundings at 2300 UTC for the analogue days number 2 and 3.

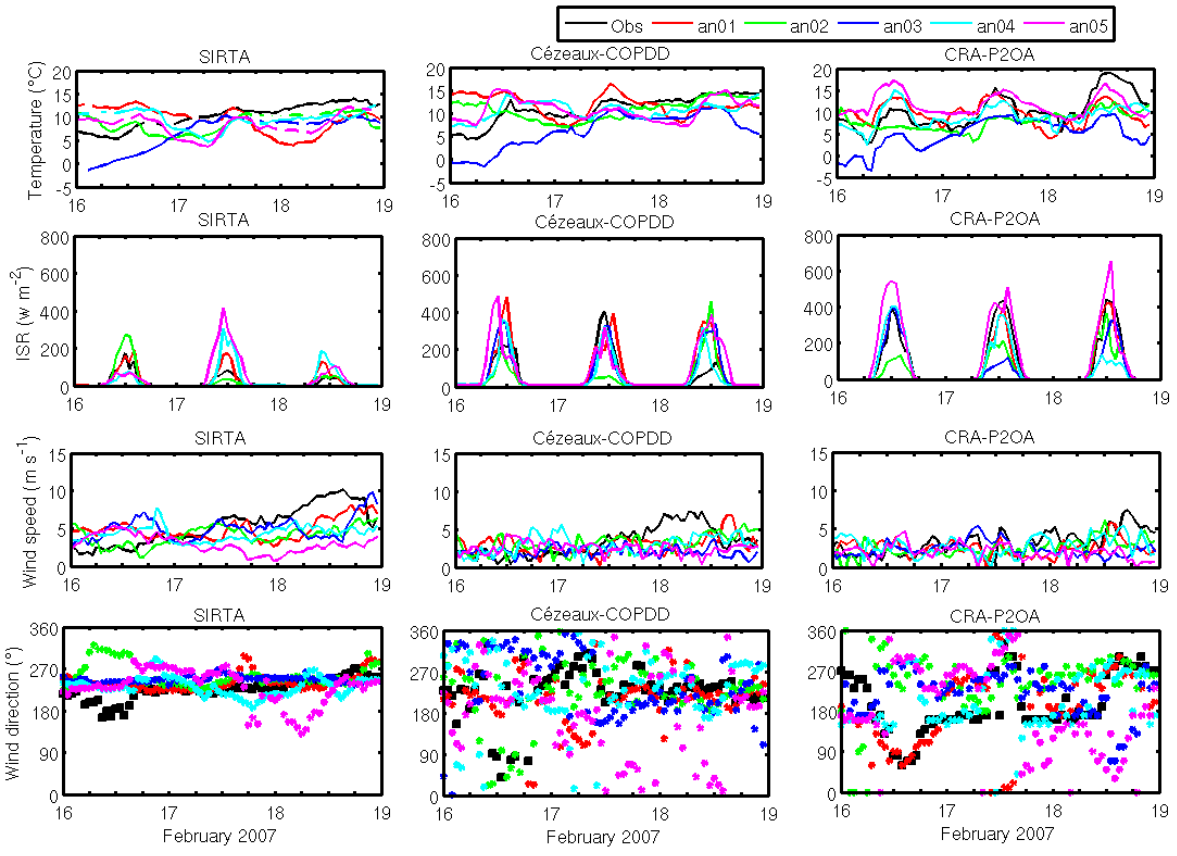

785 FIG. 10. Time series at each site of the temperature, incoming shortwave radiation (ISR), wind speed and
786 direction during the period 16 to 18 January 2007. The observed series are represented in “black”, while the
787 other colors represent the historical data of the five most accurate analogue days for 18 January 2007.

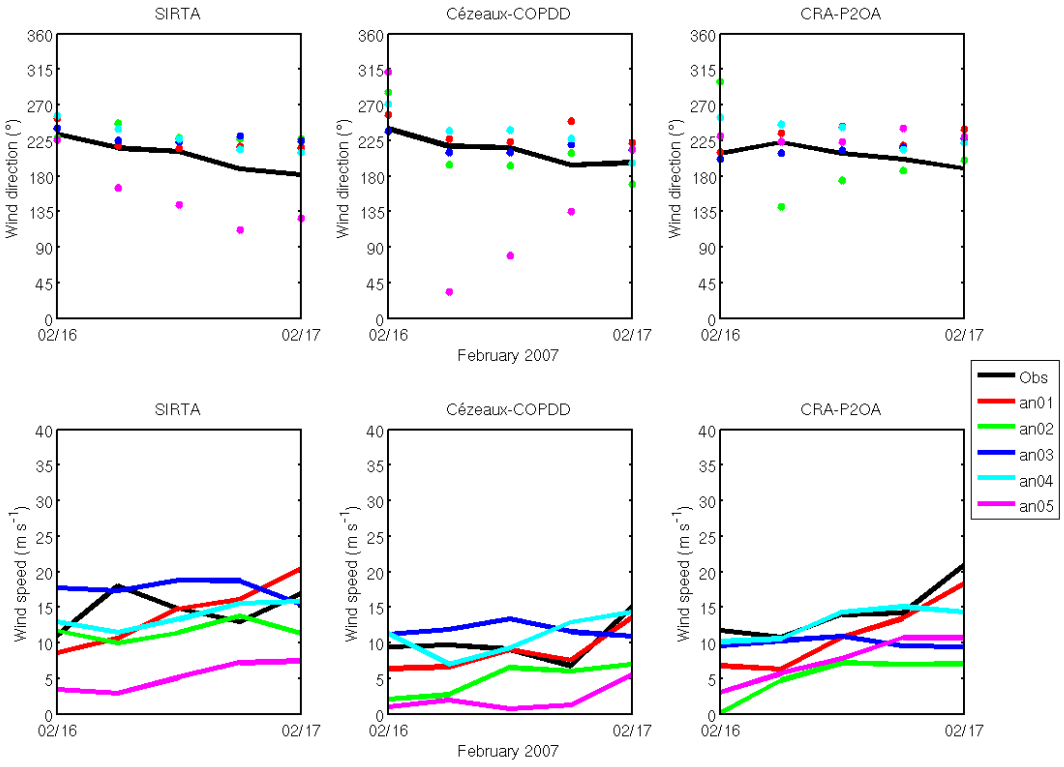

FIG. 11. As in Fig. 8 but for 16 February.

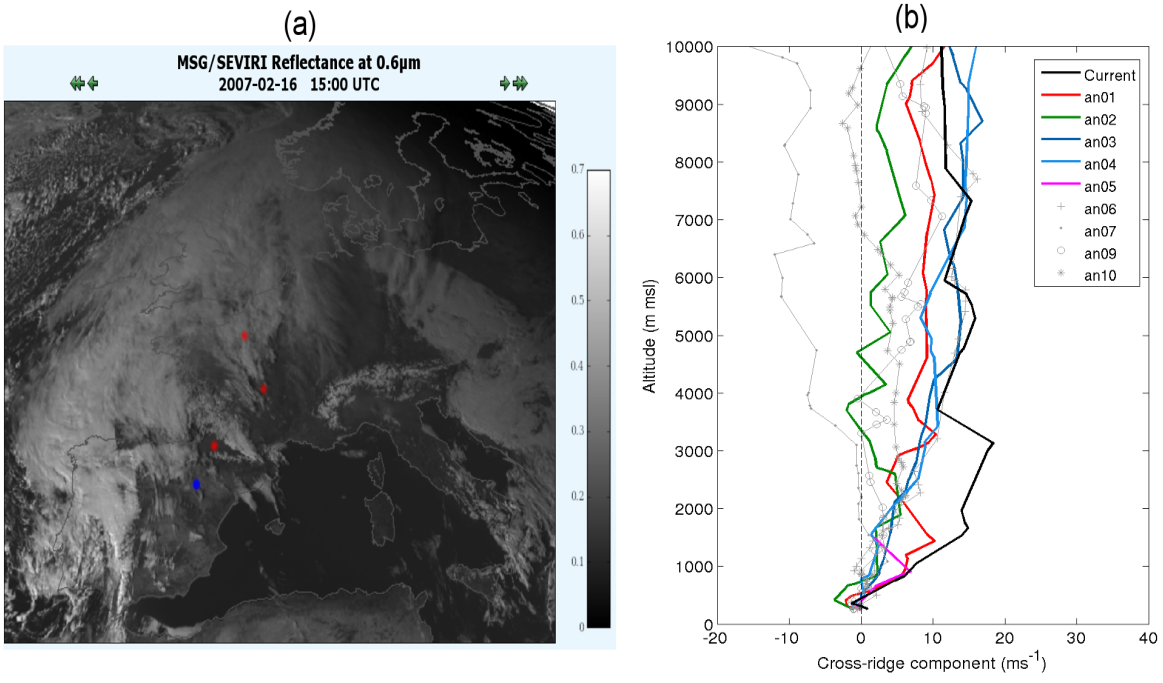

FIG. 12. (a) Reflectance in the visible channel of MSG/SEVIRI at 0.6 μm on 16 February 2007 at 1500 UTC. This picture is available on the following site: http://www.icare.univ-lille1.fr. Red points in (b) indicate the location of the three observatories; the blue point represents the radiosonde station in Zaragosa. (b) Vertical profiles of the wind component transversal to the Pyrenees ridge (210°) observed at Zaragosa, Spain, on 16 February and the entirety of its analogues, at 0000 UTC,

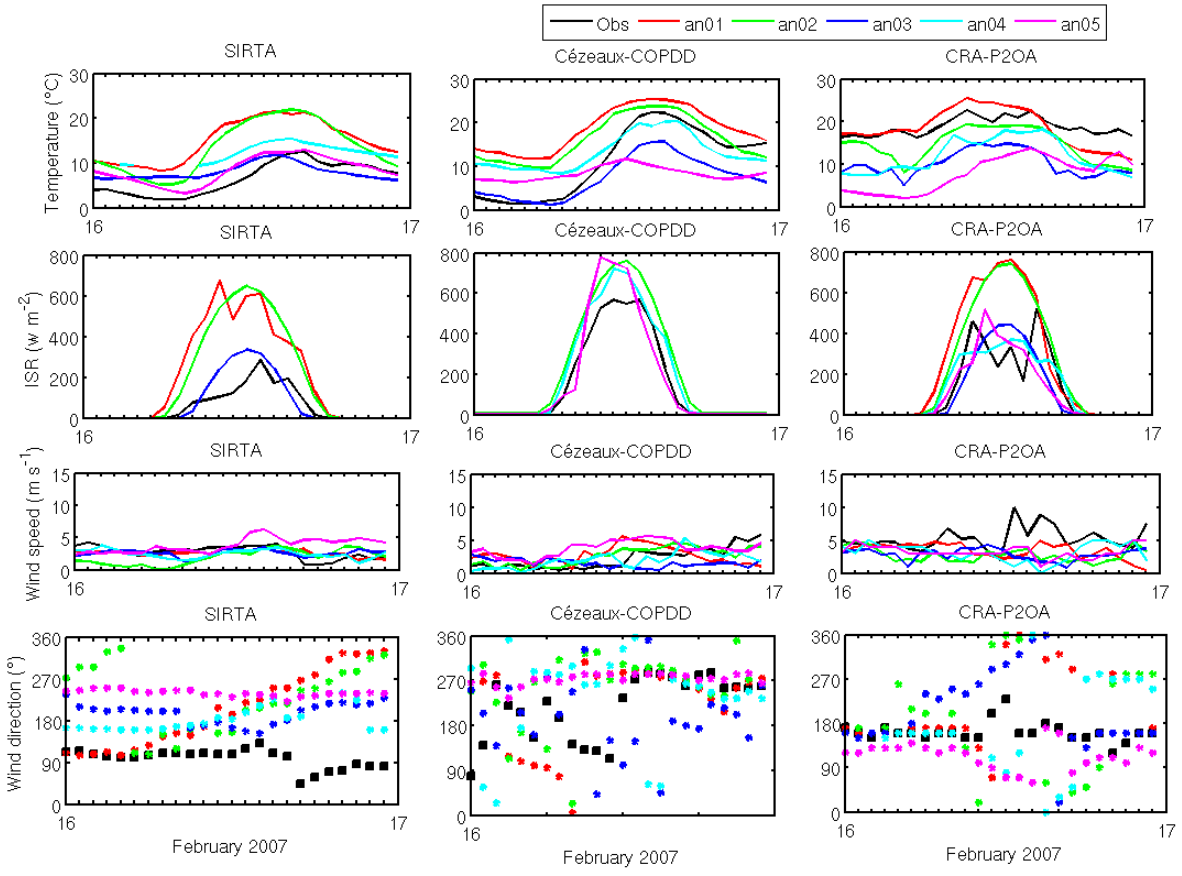

FIG. 13. As in Fig. 10 but for 16 February.